Two Muscle-Specific and Direct Transcriptional Targets of DAF-16/FOXO Activated by Reduced Insulin/IGF-1 Signaling

Shifei Wu[1,2], Yan Li[2], Charline Roy[3], Ying Wang[2], Ben Mulcahy[2], William Li[1,2], John Calarco[4], Wesley Hung[2,6], Mei Zhen[1,2,4,5,6]

[1]Department of Molecular Genetics, University of Toronto, Toronto, Canada

[2]Lunenfeld-Tanenbaum Research Institute, Mount Sinai Hospital, Toronto, Canada

[3]Université de Lyon, Université Claude Bernard Lyon 1, CNRS UMR 5284, INSERM U 1314, Institut NeuroMyoGène, MeLiS, Lyon, France

[4]Department of Cell and Systems Biology, University of Toronto, Toronto, Canada

[5]Department of Physiology, University of Toronto, Toronto, Canada

[6]Senior author

Abstract

C. elegans insulin/insulin-like growth factor 1 signaling (IIS) affects diverse physiological processes through the DAF-16/FOXO transcription factor. Despite its presence in all somatic cells, DAF-16's physiological effects, such as modulation of dauer formation, synapse maturation, axon regeneration, and adult longevity, exhibit prevalent tissue-specificity as well as tissue crosstalk. This implies that tissue-specific DAF-16 transcriptional programs contribute to the functional diversity of IIS. To further examine this possibility, we sought to identify tissue-specific and direct transcriptional targets of DAF-16 in muscle cells. Following FACS-sorting to enrich mature muscle cells from young adult animals, we compared the muscle transcriptomes under high and low IIS states, with and without DAF-16. We further analyzed and compared the DAF-16 docking sites in muscle and intestine cells from published datasets. These analyses revealed 14 potential muscle-specific DAF-16 transcriptional targets, among which we validated two that are strongly and specifically activated by DAF-16 in muscles: a secreted protein C54F6.5 and a calcium-binding protein CEX-1/Calexcitin. Both genes exhibit DAF-16-independent non-muscle expression, explaining their low rank or absence from the current DAF-16 target lists generated by multiple independent whole-animal microarray or mRNA-sequencing analyses. These results support the notion of tissue-specific DAF-16 transcriptional programs and highlight the importance of verifying FOXO targets in a cell-type-specific manner.

Introduction

From invertebrates to vertebrates, the insulin/insulin-like growth factor 1 (IGF-1) signaling (IIS) regulates a variety of physiological functions[1], from developmental decision[2–5], neural development[6–11], learning[12–17], aging[18–23], longevity[3,5,24,25], to stress response[26,27].

Key components of the canonical IIS pathway are conserved across animals (for reviews[5,28–30]). The signaling components and physiological functions of IIS have been extensively investigated in *C. elegans*. *C. elegans* exhibits a large expansion of genes encoding insulin-like (INS) ligands[31,32]. With remarkable complexity in expression pattern[33], 40 functionally redundant and specific INS ligands either positively or negatively regulate IIS activity[14,33–37]. In contrast to the expansion of INS ligands, *C. elegans* has a single, ancestral insulin/IGF-1 receptor DAF-2[3,24]. An activated DAF-2 receptor activates a conserved AGE-1/PI3[4], PDK, and AKT[38,39] kinase cascade, leading to phosphorylation and cytoplasmic retention of the DAF-16/FOXO transcription factor, inhibiting its transcriptional activity[2,12,25,40–42] (Figure 1A).

A mechanistic understanding of the role of IIS requires the identification of DAF-16 transcriptional targets. Consistent with a pan-tissue expression pattern exhibited by all examined components of the signaling cascade, from DAF-2 to DAF-16/FOXO, IIS regulates diverse biological processes. How does a single IIS cascade achieve functional specificity? The specificity of IIS in part comes from 40 INS ligands expressed from specific and overlapping tissues[37]. DAF-16 may also define tissue-specific functions of IIS by activating tissue-specific transcriptional targets.

Indeed, several processes regulated by IIS activity exhibit prominent tissue-specificity. A decreased IIS activity leads to increased adult lifespan[3,5,24,25], and promotes an alternative 'dauer' developmental state that confers resistance to starvation and dehydration[2–5]. Both processes depend on increased DAF-16 activity in the intestine. DAF-16 functions through interneurons to affect salt-associated learning[12–17]. In motor neurons, decreased IIS and DAF-16 activation functions intrinsically to delay age-related decline in axon regeneration[43]. Age-dependent motility decline appears to be contributed by IIS from both neurons and muscles, in opposite ways at different phases of adults[21,44].

DAF-16 regulates many physiological processes in muscles, including muscle arm extension[45], neuromuscular junction development[34], prevention of cell death[46], and resistance to

heat-induced calcium overload[47]. DAF-16 plays both cell autonomous and non-autonomous roles in the muscle cells, consistent with observations in other tissues[48]. Cell-autonomous functions of DAF-16 can be explained by DAF-16 directly regulating transcriptional targets; on the other hand, DAF-16 might mediate inter-tissue communication through targets that are secreted or surface molecules to indirectly affect the development of other cells.

Most efforts to identify DAF-16 targets focused on measuring differential gene expression in the presence or absence of active DAF-16 in whole worms, using either microarrays or mRNA-sequencing (mRNA-seq). This has led to the identification of transcriptional changes associated with metabolism, oxidative-stress response, lifespan, and development[49–53]. Towards the identification of tissue-specific DAF-16 targets, a recent transcriptome profiling on all neuronal cells identified panneurally-enriched targets, one of which was shown to participate in axon regeneration and learning[54]. In general, however, there is a lack of comprehensive information on direct DAF-16 targets in a cell-type-specific manner.

We began this effort with the body wall muscle cells, motivated in part by the abundance and homogeneity of this tissue, and in part by the availability of raw DAF-16 ChIP-sequencing (ChIP-seq) data in muscle cells[55]. We combined muscle-specific mRNA-seq and muscle/intestine-specific ChIP-seq datasets to identify high-confidence, muscle-enriched, and direct DAF-16 transcriptional targets. We validated the muscle-specific, DAF-16-dependent expression of the top two candidates by this method. Identification of cell-specific and direct transcriptional targets of DAF-16 addresses how the IIS regulates diverse physiological processes in different cells.

Results

The experimental setup to compare DAF-16-dependent transcriptional changes under high and low IIS states in mature muscle cells

We used mature animals of four different genetic backgrounds — wildtype, *daf-16(lf)*, *daf-2(lf)*, and *daf-16(lf); daf-2(lf)* — to model two different IIS states, and to compare DAF-16-dependent transcript changes under the high and low IIS states separately (Figure 1B).

Under the high IIS state, DAF-16 is maintained at the cytosol thus with low activity in transcriptional regulation. We compared transcriptomes of wildtype animals and *daf-16(lf)* mutants, from synchronized cultures raised at optimal laboratory conditions (22.5ºC). Reduced

IIS induces nuclear translocation of DAF-16 and activation of its transcriptional activity. Under the low IIS state, we compared the transcriptomes between *daf-2(lf)* and *daf-16(lf); daf-2(lf)* mutant animals. Since *daf-2(lf)* larvae arrest reproductive development, we raised *daf-2(ts)* larvae at the permissive temperature (15ºC) until after the last molting, followed by moving them to the non-permissive temperature (22.5ºC) for 8 hr to allow inactivation of DAF-2 (Methods).

To uncover muscle-enriched changes in mature animals, we FACS-sorted muscle cells that were labeled by GFP and dissociated from young adults ('muscle cells'). Three to four replicas, each with 20,000-40,000 sorting events, were obtained for each genotype. Non-GFP-enriched cells ('all cells') were collected from each sample after undergoing dissociation and FACS-sorting but without GFP gating as controls for muscle-enriched transcripts, as well as for transcriptional changes induced by experimental procedures (Figure 1B).

In subsequent analyses, we referred both the absence of DAF-16 and high IIS-induced low DAF-16 activity as 'inactive DAF-16' samples, whereas low IIS-induced high DAF-16 activity as 'active DAF-16' samples.

No DAF-16-dependent transcriptional changes under the high IIS state in mature muscle cells

Under the high IIS state (wildtype animals and *daf-16(lf)* mutants), muscle transcriptomes had little changes in the presence or absence of DAF-16. There were only 11 statistically significant differentially expressed genes (FDR < 0.05, n = 4 replicas) (Figure 1C). All candidates were of low abundance in both wildtype and *daf-16* muscle cells, and they are thus unlikely to be high-confidence DAF-16 regulated genes (Table 1).

An overall negative outcome is expected when DAF-16's activity is maintained low and when experimental manipulation did not induce acute stress responses in wildtype muscles. This negative result is also consistent with findings from previous whole-animal mRNA-seq analyses, where under non-stressful culture conditions, there were no appreciable transcriptional differences[23,53]. Thus, under non-stressful culture conditions, DAF-16 activity is maintained at a low level in muscle cells.

195 candidates for DAF-16-dependent up and down-regulation in mature muscle cells

Transcriptional modulation by DAF-16 occurs under the low IIS state. Consistently, comparing the transcriptome between *daf-2(lf)* muscle cells and *daf-16(lf); daf-2(lf)* muscle cells, we obtained 312 statistically significant DAF-16-dependent expression changes (FDR < 0.05, n = 3 replicas) (Figure 1D). Among them, 142 were upregulated and 170 were downregulated (Table 2 and S1). We considered these genes candidates for DAF-16-dependent transcriptional regulation.

To identify the most consistent transcriptional changes induced by reduced IIS, we further filtered the gene list against two control transcriptomes with inactive DAF-16, the muscle transcriptomes of wildtype animals and *daf-16(lf)* mutants under the high IIS state. This reduces the list to 195 candidates, 88 upregulated and 107 downregulated genes, when DAF-16 is active (Table 2 and S2). By incorporating three different genotypes for inactive DAF-16 controls, we aimed to reduce noises from stochastic compensatory events and the small number of experimental replicas for the bulk mRNA-seq analyses.

139 candidates for muscle-enriched DAF-16-dependent regulation

From the 195 candidates, we next sought those that are preferentially regulated in muscle cells by comparing the transcript abundance between *daf-2* sorted ('muscle cells') and non-sorted ('all cells') samples, both with active DAF-16. Among them, 152 showed enrichment or depletion in muscle cells, whereas the remaining 43 exhibited similar abundance for both muscle cells and 'all cells'. Including 'all cells' with inactive DAF-16 (wildtype and *daf-16(lf)*) as additional filters, we obtained 139 candidates — 62 upregulated and 77 downregulated genes — preferentially regulated in muscle cells (Figure 2, Table 2 and S2). Although a transcriptional regulation shared by the muscle and non-muscle cells does not exclude its involvement in muscle-specific functions, we chose to focus further analyses on the smaller set of candidates for identifying and validation of candidates with a high likelihood for muscle-dependent functions.

Two candidate muscle-specific and direct DAF-16 transcriptional targets

Transcription factors can affect the transcriptome directly, by binding near genes and activating or repressing transcription, or indirectly by modulating expression of secondary transcription factors. We sought to limit our analyses to direct transcripts of DAF-16 by considering the DAF-16-docking sites revealed by tissue-specific ChIP-seq analyses.

We previously generated the *daf-16(lf); daf-2(lf)* strains where a single-copy insertion of functional GFP::DAF-16a restored DAF-16 expression specifically in either the intestine or the muscle cells[35] to generate GFP::DAF-16a-ChIP-seq reads[55]. The DAF-16a isoform was chosen because this, but not the other (b, d/f) isoforms, was required in muscles for neuromuscular junction maturation[34]. From these reads, we mapped 1919 DAF-16a docking sites in the muscle-specific GFP::DAF-16a strain, and 955 and 2422 docking sites in two independent intestine-specific GFP::DAF-16a strains. Binding peaks spanned all six chromosomes without obvious patterns (Figure 3). The large and variable docking sites are consistent with previous findings that only a small fraction of DAF-16 docking events leads to activated transcriptional activation[56].

Among the 139 candidates, 55 showed GFP::DAF-16a docking within 5 kb upstream of the transcription start site or 5 kb downstream of the stop codon. Among them, 43 are upregulated and 12 are downregulated by activated DAF-16 (Table S3). We then further filtered the list of genes for those whose upstream or downstream 5 kb regions were occupied by GFP::DAF-16a docking sites in muscles but not in intestines. This resulted in 14 candidates whose docking sites are absent from both intestine-specific GFP::DAF-16a ChIP-seq datasets, all of which except one are upregulated by activated DAF-16.

We ranked the 14 candidates for DAF-16 muscle-specific and direct targets by the fold change in animals with or without DAF-16 under the low IIS state. After taking the relative abundance and deviation in fold changes into consideration, only two top candidates (*C54F6.5* and *cex-1)* remain (Table 3). Both *C54F6.5* and *cex-1* possess DBE, a DAF-16-binding site for direct transcriptional regulation[49,56,57]. Both candidates were ranked low[57] for DAF-16-dependent transcriptional changes from current whole-animal studies.

DAF-16 upregulates C54F6.5, a secreted small protein, specifically in muscle cells

C54F6.5 is predicted to encode a *C. elegans* specific, functionally uncharacterized and secreted 56aa protein[58]. With close to 0 reads in the inactive DAF-16 muscle samples and over 45-fold changes in the active DAF-16 samples (Figure 4A), DAF-16 might upregulate *C54F6.5* predominantly in muscles.

Because our mRNA-seq datasets were obtained from dissociated cells, we thought it is important to verify top candidates using RNA samples independently prepared from intact *C.*

elegans samples and strains without transgenic markers. Using total mRNA from synchronized and age-matched wildtype, *daf-2(lf)*, *daf-16(lf)*, and *daf-16(lf); daf-2(lf)* young adults cultured in conditions similar to that of mRNA-seq experiments, we quantified the transcript level using RT-qPCR (Figure 4B, Figure S1). We reason that an upregulation should be detectable in total RNA since the upregulation of *C54F6.5* transcripts was already observed in *daf-2(lf)* and *daf-16(lf); daf-2(lf)* 'all cells' samples. Indeed, our RT-qPCR analyses recapitulated DAF-16-dependent, robust upregulation of *C54F6.5* transcripts in *daf-2(lf)* mutants.

We sought to verify the muscle-specificity of DAF-16-dependent *C54F6.5* transcription using transcriptional and translational reporters. Immediately upstream of *C54F6.5*'s coding region contains a muscle-specific peak of DAF-16a binding site that contains DBE, a consensus DAF-16-binding element (Figure 4C). Both transcriptional and translational reporters that include this region revealed DAF-16-dependent muscle expression as well as DAF-16-independent expression in the spermatheca (Figure 4D, E).

In wildtype animals, the transcriptional reporter showed sporadic weak muscle signal, which was eliminated in *daf-16(lf)* mutants. *daf-2(lf)* mutant animals showed consistent and robust muscle GFP signals, whereas *daf-2(lf); daf-16(lf)* animals exhibited a similar pattern to that of wildtype animals, with even less leaky muscle signals. The translational reporter, driven by the same promoter but with its full coding sequence fused in-frame with GFP showed the same trend (data not shown). Moreover, in the DAF-16-active *daf-2(lf)* mutants, *C54F6.5::GFP* was present not only in muscle cells but also coelomocytes (Figure 4F), the scavenger cell where secreted proteins accumulate[59], consistent with *C54F6.5* being a secreted protein.

In the spermatheca, across four genotypes, both reporters showed consistent and strong GFP signals (Fig. 4C and data not shown). DAF-16-independent expression in spermatheca might indicate an IIS-independent expression of the gene or a less physiological expression pattern revealed by a promoter fragment in a non-endogenous genomic context.

DAF-16 upregulates CEX-1/Calexcitin, a Ca^{2+} binding protein, specifically in muscle cells

Using both RT-qPCR and reporter analyses, we similarly confirmed that *cex-1* is upregulated by DAF-16 specifically in muscle cells (Figure 5A, B; Figure S1).

Finding muscle-specific and DAF-16-dependent expression of *cex-1* was a surprise because a fragment of the *cex-1* promoter has long been used to drive constitutive expression in a

single pair of interneuron RIM[60,61]. Our ChIP-seq analyses revealed a DBE consensus binding site in *cex-1*'s 3' UTR that was only occupied in muscle cells (Figure 5C). Indeed, including a 3' UTR fragment with this site in the *cex-1* reporter revealed an expression pattern consistent with the RNA-seq. analyses: a DAF-16-independent, constitutive expression in the RIM neurons (arrowheads, Figure 5D), and a DAF-16-dependent upregulation of expression in muscle cells between wildtype animals and *daf-2(lf)* mutants (Figure 5D-E). This reporter expression pattern is also consistent with the higher *cex-1* read counts in the wildtype 'all-cell' samples than for *C54F6.5*.

Ambiguity of remaining 12 candidates

We further considered the candidacy of the remaining candidate muscle-specific DAF-16 targets. Compared to *C54F6.5* and *cex-1*, they had either low reads or smaller differences in expression between the DAF-16-active and -inactive conditions; all with higher variability, making them low-confidence candidates.

We examined this idea by testing *gstk-2* with a GFP reporter expressed from the endogenous locus (Figure S2). We selected this gene because it showed a similar degree of mean fold change to *cex-1* and has a muscle-specific, DBE-containing DAF-16 docking, but with an estimated >10-fold lower than both *C54F6.5* and *cex-1* (Table 3). We observed low, but consistent GFP signals in body wall muscles, pharyngeal cells, and the epithelial seam cells across wild-type, *daf-16(lf)*, *daf-2(lf)*, and *daf-16(lf); daf-2(lf)* animals (Figure S2). The negative result from this validation supports our criteria to exclude the remaining 12 candidates.

Discussion

Physiological functions of IIS exhibit strong tissue-specificity, and DAF-16 exhibits both cell autonomous and non-autonomous functions. However, tissue-specific and direct DAF-16 targets remain largely unexplored. Combining tissue-specific mRNA-seq, ChIP-seq, transgenic reporters, and whole animal RT-qPCR, we identified two muscle-specific and direct transcriptional targets upregulated by DAF-16 induced by reduced IIS. They represent <1% of the total number of genes (195) that showed DAF-16-dependent transcriptional changes. Our GO-term analyses showed that the majority of DAF-16-dependent transcriptional upregulation in muscle cells are enriched for glutathione transferase activity, structural constituent of cuticle,

antioxidant activity, and oxidoreductase activity — a subset of enriched terms from DAF-16 upregulated genes in *daf-2(lf)* all cell samples. Neither C54F6.5 nor CEX-1 are included by these terms, further supporting their muscle-specific functions. Validation of these two candidates suggests that whole-animal transcriptome profiling may have overlooked tissue-specific DAF-16 targets with tissue-specific physiological functions. These analyses serve as the 'rules-of-thumb' guide to gauge the potential relevance of differential gene expression revealed by the small number of replicas of the bulk mRNA-seq analyses.

Potential physiological functions of C54F6.5

The function of both muscle-specific DAF-16 targets in IIS-mediated physiological processes remains unclear. *C54F6.5* showed robust transcriptional activation in muscle cells when DAF-16 is active, similar to *sod-3*, the top, pan-tissue effector of DAF-16. It encodes a secreted protein consisting of 56 amino acids. Like many predicted small, secreted proteins, C54F6.5 is considered to be nematode-specific by sequence homology. Nematode-specific secreted small proteins are enriched for regulation upon exposure to pathogens and have been proposed to underlie the *C. elegans* immune response[62,63]. C54F6.5 might constitute a component of defense mechanisms contributed by muscle cells. We previously identified an IIS-dependent retrograde signaling from muscle cells to attenuate presynaptic development of motor neurons[34]; it is possible that C54F6.5 may be part of the retrograde signaling. Interestingly, the activity of GABAergic motor neurons has been associated with maintained adult motility[64] and recently with innate immune responses to pathogens[65]. The physiological outcome of these two different processes might be related at the molecular level.

The lack of C54F6.5 homologs based on the primary sequence alignment does not implicate that it engages a nematode-specific signaling pathway. We do not have widely accessible and reliable tools to predict the structural similarity among small secreted proteins. Indeed, while amino acid sequences for the bulk of the *C. elegans* neuropeptides revealed no homologs, thus deemed 'nematode-specific', several have been shown to bind and activate evolutionarily conserved GPCR signaling and to serve homologous physiological functions[66,67].

Potential physiological functions of CEX-1

cex-1 encodes the *C. elegans* homolog of a conserved protein family calexcitin. With three Ca^{2+}-binding EF-hand domains, calexcitin is a regulator of neuronal activity implicated in learning[68–70]. Mechanistically, it is a proposed Ca^{2+} sensor that modulates membrane excitability via the K^+ channel and ryanodine receptor activity in a Ca^{2+}-dependent manner[68]. Interestingly, calexcitin was recently shown to bind the ryanodine receptors in the sarcoplasmic reticulum[71].

Given the popularity of the *cex-1* promoter, and its usage to dissect the role of the RIM inter-neurons' role in *C. elegans* associative learning and decision-making[72–74], and the neuronal activation-induced stress response[61], it is a bit surprising that there has been no reported functional study on the *cex-1* gene itself. Revealing its muscle-specific transcriptional activation by DAF-16 promotes several hypotheses on its potential role in aging-dependent physiological functions. For example, CEX-1 might contribute to the known effects of IIS on the age-dependent maintenance of muscle activity and muscle survival[44,46]. Intriguingly, impaired ryanodine receptor activity and reduced IIS have been reported to reduce heat shock-induced Ca^{2+} overload in muscle cells[47]. DAF-16-mediated activation of *cex-1* expression may contribute to the Ca^{2+} overload through potentiating the ryanodine receptor activity.

Towards tissue-specific targets: strength and weakness of our approach

Our approach applies a series of increasingly stringent criteria to select high-confidence muscle-specific DAF-16 direct transcriptional targets. Validation of our top candidates, both being the overlooked targets by whole animal studies, lends strong support to a tissue-specific and stringent approach.

Our final list is very small, and the two that we validated were the only high-confidence candidates when we considered the consistency and size of differential expression. We do not have sufficient data to evaluate whether the short list reflects a physiological phenomenon, where a small handful of molecular drivers underlie tissue-specific functions, or whether the excessively stringent criteria have excluded more direct DAF-16 transcriptional targets with potential relevance to muscle cells. Empirically, we favored the second possibility for the following reasons.

First, our selection for muscle enrichment of transcriptional regulation by DAF-16 and muscle-specific docking by DAF-16a assumes that they enrich for genes being functionally

important in muscle cells. This might apply for most, but certainly not for all genes of critical physiological functions, especially those with low abundance.

Second, we do not have the objective criteria to evaluate the quality, depth, and functional relevance of the ChIP-seq data. We noted that the sequential filtering with the muscle-enriched transcriptomics analyses maintained many high-confidence DAF-16 targets identified in previous whole-animal studies[49,54,57]. Many such candidates are removed when we incorporated the first filter from the muscle ChIP-seq data. In fact, considering the presence of a docking site of muscle GFP::DAF-16a removed ~2/3 of candidates, including *sod-3*, which we considered a gold standard and subsequently applied as the positive control for RT-qPCR analyses (Figure S1). The exclusion of isoforms other than DAF-16a may explain why *sod-3* was not included. It is also possible that those ChIP-seq experiments, when carried out as part of a large-scale study for many transcription factors, were not as carefully controlled for developmental stages or genome coverage[55] as for the mRNA-seq experiments. In addition, scanning for DAF-16a docking within the 5kb flanking the beginning and end of the coding region, although being expanded from known regions enriched for the DBE-consensus DAF-16 site, is simply an arbitrary criterion. Lastly, we should not assume that all DAF-16's direct targets will exhibit detectable DAF-16a docking for transcriptional regulation.

Future directions

We propose two follow-up studies. First, to investigate the physiological functions of C54F6.5 and CEX-1 in the context of the IIS. As outlined in previous sections, phenotypical analyses of the respective knockout mutants, such as age-related motility, muscle physiology, and pathogen resistance, serve as an excellent starting point. A requirement of either gene in the phenotypes of *daf-2(lf)* mutants, and if so, their sufficiency to bypass the presence of DAF-16 for the respective *daf-2(lf)* mutant phenotype can be determined by standard molecular genetic studies, e.g. transgenic and tissue-specific rescues or deletion.

Second, to evaluate the validity to incorporate ChIP-seq data for future studies of DAF-16/FOXO or other transcription factors, the 139 candidates obtained from the mRNA-seq analyses alone should be independently evaluated for DAF-16-dependent transcriptional regulation. Ideally, a systematic, endogenous genomic tagging of these genes will provide the needed assessment of the quality, coverage, and validity to incorporate information from the

ChIP-seq in search for cell-type specific and direct targets. Lastly, a systematic, single-molecular FISH of the 139 candidates will provide the ultimate quantitative assessment of the quality and coverage of the mRNA-seq datasets.

Methods

Strains and transgene generation

C. elegans strains were cultured on OP50-seeded NGM media[75] at 22.5°C (unless otherwise stated). *daf-2(e1370)* temperature-sensitive animals were cultured at the permissive temperature 15°C and shifted to the restrictive temperature for experiments (see below for details). A list of strains used in this study is provided in Table S4.

Transgenic animals were generated by microinjection as described previously[76]. A stable extrachromosomal array of each reporter was generated and then crossed into *daf-16(lf), daf-2(lf), daf-16(lf); daf-2(lf)* afterward.

Transcriptional and translational reporter plasmid construction

C54F6.5: For the transcriptional reporter, the promoter sequence (1225 bp upstream of its start codon and the first 106 bp of its coding sequence) was generated with PCR from wild-type genomic DNA and subcloned into Fire Vector 1997 to create pJH4768. The Fire Lab *C. elegans* Vector Kit was a gift from Andrew Fire (Addgene kit # 1000000001). A translational reporter was later generated by synthesizing the remainder of the coding sequence (IDT) and introducing it into pJH4768 by Gibson Assembly to generate pJH4815.

cex-1: A previously described P*cex-1* mCherry reporter for RIM labeling, which contains 2862 bp upstream of its start codon[77], was used to create pJH4782. *cex-1* 3' UTR (1053 bp downstream of its stop codon) was generated with PCR from genomic DNA and used to replace the *unc-54* 3' UTR in the original vector.

FACS isolation of muscle cells and mRNA-seq preparation

Wild-type and *daf-16(lf)* worms with GFP-labeled muscles (Table S4, JAC127 and ZM9156) were synchronized and grown at 22.5°C throughout development until they became young adults. *daf-2(lf)* and *daf-2(lf); daf-16(lf)* worms with GFP-labeled muscles (Table S1, ZM10379 and ZM10380) were synchronized and grown at 15°C until L3 to prevent dauer

formation in *daf-2(lf)* worms and shifted to 22.5°C to activate DAF-16 until they became young adults. From these synchronized young adult worms, cells were extracted with SDS-DTT, dissociated with pronase, and filtered through a 20 µm cell strainer (adapted from[78]). FACS analysis was performed to isolate GFP positive and propidium iodide (PI) negative muscle cells. A fraction of PI negative cells was 'sorted' without GFP gating as the "all cells" control sample. 20,000-40,000 sorting events were performed for each strain (which typically yielded ~20X coverage). We performed four independent replicas for the wildtype and *daf-16(lf)* set; and three independent replicas for the *daf-2(lf)* and *daf-16(lf); daf-2(lf)* set. RNA was extracted with TRIzol, cleaned up with DNAse I, and quality checked before being sent for sequencing (adapted from[78]). In parallel, aliquots of sorted muscle and all cells were plated, and muscle cell enrichment was confirmed.

Analysis of mRNA-seq data

mRNA-seq raw reads were processed to produce transcript abundance and counts with Salmon 1.4.0. Differential gene expression analysis was performed with DESeq2. Results were verified with STAR and HTSeq to examine the validity of estimated read maps from Salmon. GraphPad Prism and Pheatmap were used for visualizing abundance data.

Analysis of ChIP-seq data

ChIP-seq raw data were obtained for XE1464 (ENCFF281NRH, ENCFF657MHD, ENCFF229JKH, ENCFF023XDP), ZM7247 (ENCFF004HMK, ENCFF018WCD, ENCFF889RBK), and ZM8745 (ENCFF288VDV, ENCFF846OUT, ENCFF963PAM) from a publicly available database[55]. To identify muscle and intestinal DAF-16 docking sites, these ChIP-seq raw reads were aligned with Bowtie 2 2.4.1 and further processed with SAMtools. Then peaks were called with MACS2 for each replicate using the input ChIP-seq data without antibody enrichment for DAF-16 binding sequences. Lastly, peaks from two replicates were combined with IDR. ChIPseeker was used to map peaks to genes that are within 5 kb of the peak. IGV was used to visualize binding sites for individual genes. chromoMap was used to visualize binding sites genome-wide.

RT-qPCR

Animals were synchronized and cultured as for those used for mRNA-seq analyses. Total RNA was extracted from synchronized young adult worms using TRIzol and with the method described previously[78]. RT-qPCR was performed with Luna Universal One-Step RT-qPCR Kit from NEB on BioRad CFX96 Touch Real-Time PCR Detection System. Each RNA sample was tested with gene-specific primers (see Table S5 for sequences). We used two housekeeping genes whose expression is not dependent on IIS as controls for expression. *pmp-3* has been previously described[79]. *rpl-17* was chosen because its transcript level is high and consistent in all of our samples based on our RNA-seq data. Each RT-qPCR experiment was performed using 4 different dilutions of extracted RNA from each sample. The experiment was repeated 3 times. The relative fold expression change was calculated using the $2^{-\Delta\Delta CT}$ method. Specifically, at each concentration, the ΔCt between the gene of interest and *rpl-17* or *pmp-3* was calculated for all genes and for all samples. At each concentration, the ΔΔCt and thus fold expression change was then calculated between the wild-type sample and other samples.

Statical analysis for RT-qPCR comparison and fluorescence intensity comparison was performed by one-way ANOVA. Dunnett's multiple comparisons test was done for pairwise comparison between wild-type and other genotypes.

Confocal fluorescent microscopy

Worms were cultured at 20°C until L4, from which transgenic worms were picked and shifted to 22.5°C until they became young adults. These synchronized young adults were immobilized on dry 2% agarose pads under coverslips. Images were acquired using a 20x or 60x objective on a Nikon Ti2 spinning disk confocal microscope equipped with an Andor Zyla VSC-07720 camera. Using the software NIS elements, large images were taken with 15% overlap, and Z-stacks were acquired at a step size of 2 μm (20x objective) or 1 μm (60x objective). The maximum projection was shown. For each transgenic line, imaging and processing conditions were kept constant. Quantification was performed with ImageJ 2.3.0[80].

Author contributions M.Z. conceptualization; M.Z., J.C. supervision; S.W., W.H. experimental design, data collection, and analyses; Y.L., C.R., Y.W., B.M., W. L., J.C. reagents and data collection; S.W. Visualization; S.W., M.Z draft; W.H., B.M. editing. M.Z. funding.

Acknowledgments We thank the Natural Sciences and Engineering Research Council of Canada RGPIN2017-06738 (to M.Z.) and USRA (to S.W.) for funding. Kin Chan, Arneet Saltzman, and Tammy Lee for advice on RNA-seq, ChIP-seq, and RT-qPCR.

References

1. Rask-Madsen, C. & Kahn, C. R. Tissue–Specific Insulin Signaling, Metabolic Syndrome, and Cardiovascular Disease. *Arterioscler. Thromb. Vasc. Biol.* **32**, 2052–2059 (2012).
2. Gottlieb, S. & Ruvkun, G. daf-2, daf-16 and daf-23: genetically interacting genes controlling Dauer formation in Caenorhabditis elegans. *Genetics* **137**, 107–120 (1994).
3. Kimura, K. D., Tissenbaum, H. A., Liu, Y. & Ruvkun, G. daf-2, an insulin receptor-like gene that regulates longevity and diapause in Caenorhabditis elegans. *Science* **277**, 942–946 (1997).
4. Morris, J. Z., Tissenbaum, H. A. & Ruvkun, G. A phosphatidylinositol-3-OH kinase family member regulating longevity and diapause in Caenorhabditis elegans. *Nature* **382**, 536–539 (1996).
5. Kaletsky, R. & Murphy, C. T. The role of insulin/IGF-like signaling in C. elegans longevity and aging. *Dis. Model. Mech.* **3**, 415–419 (2010).
6. Man, H. Y. *et al.* Regulation of AMPA receptor-mediated synaptic transmission by clathrin-dependent receptor internalization. *Neuron* **25**, 649–662 (2000).
7. Mielke, J. G. *et al.* A biochemical and functional characterization of diet-induced brain insulin resistance. *J. Neurochem.* **93**, 1568–1578 (2005).
8. Klöckener, T. *et al.* High-fat feeding promotes obesity via insulin receptor/PI3K-dependent inhibition of SF-1 VMH neurons. *Nat. Neurosci.* **14**, 911–918 (2011).
9. Plum, L. *et al.* Enhanced PIP3 signaling in POMC neurons causes KATP channel activation and leads to diet-sensitive obesity. *J. Clin. Invest.* **116**, 1886–1901 (2006).
10. Nieto-Estévez, V., Defterali, Ç. & Vicario-Abejón, C. IGF-I: A Key Growth Factor that Regulates Neurogenesis and Synaptogenesis from Embryonic to Adult Stages of the Brain. *Front. Neurosci.* **10**, 52 (2016).
11. Chiu, S.-L. & Cline, H. T. Insulin receptor signaling in the development of neuronal structure and function. *Neural Develop.* **5**, 7 (2010).
12. Lin, C. H. A. *et al.* Insulin signaling plays a dual role in Caenorhabditis elegans memory acquisition and memory retrieval. *J. Neurosci. Off. J. Soc. Neurosci.* **30**, 8001–8011 (2010).
13. Tomioka, M. *et al.* The Insulin/PI 3-Kinase Pathway Regulates Salt Chemotaxis Learning in Caenorhabditis elegans. *Neuron* **51**, 613–625 (2006).
14. Chen, Z. *et al.* Two insulin-like peptides antagonistically regulate aversive olfactory learning in C. elegans. *Neuron* **77**, 572–585 (2013).
15. Kodama, E. *et al.* Insulin-like signaling and the neural circuit for integrative behavior in C. elegans. *Genes Dev.* **20**, 2955–2960 (2006).
16. Oda, S., Tomioka, M. & Iino, Y. Neuronal plasticity regulated by the insulin-like signaling pathway underlies salt chemotaxis learning in *Caenorhabditis elegans*. *J. Neurophysiol.* **106**, 301–308 (2011).
17. Tomioka, M., Naito, Y., Kuroyanagi, H. & Iino, Y. Splicing factors control C. elegans behavioural learning in a single neuron by producing DAF-2c receptor. *Nat. Commun.* **7**, 11645 (2016).
18. Pan, C.-L., Peng, C.-Y., Chen, C.-H. & McIntire, S. Genetic analysis of age-dependent defects of the Caenorhabditis elegans touch receptor neurons. *Proc. Natl. Acad. Sci. U. S. A.* **108**, 9274–9279 (2011).
19. Tank, E. M. H., Rodgers, K. E. & Kenyon, C. Spontaneous age-related neurite branching in Caenorhabditis elegans. *J. Neurosci. Off. J. Soc. Neurosci.* **31**, 9279–9288 (2011).

20. Toth, M. L. *et al.* Neurite sprouting and synapse deterioration in the aging Caenorhabditis elegans nervous system. *J. Neurosci. Off. J. Soc. Neurosci.* **32**, 8778–8790 (2012).
21. Hahm, J.-H. *et al.* C. elegans maximum velocity correlates with healthspan and is maintained in worms with an insulin receptor mutation. *Nat. Commun.* **6**, 8919 (2015).
22. Liu, J. *et al.* Functional aging in the nervous system contributes to age-dependent motor activity decline in C. elegans. *Cell Metab.* **18**, 392–402 (2013).
23. Li, S. *et al.* DAF-16 stabilizes the aging transcriptome and is activated in mid-aged Caenorhabditis elegans to cope with internal stress. *Aging Cell* **18**, e12896 (2019).
24. Kenyon, C., Chang, J., Gensch, E., Rudner, A. & Tabtiang, R. A C. elegans mutant that lives twice as long as wild type. *Nature* **366**, 461–464 (1993).
25. Ogg, S. *et al.* The Fork head transcription factor DAF-16 transduces insulin-like metabolic and longevity signals in C. elegans. *Nature* **389**, 994–999 (1997).
26. McColl, G. *et al.* Insulin-like Signaling Determines Survival During Stress via Post Transcriptional Mechanisms in C. elegans. *Cell Metab.* **12**, 260–272 (2010).
27. Rasulova, M. *et al.* Elevated Trehalose Levels in C. elegans daf-2 Mutants Increase Stress Resistance, Not Lifespan. *Metabolites* **11**, 105 (2021).
28. Kenyon, C. J. The genetics of ageing. *Nature* **464**, 504–512 (2010).
29. Kleemann, G. A. & Murphy, C. T. The endocrine regulation of aging in Caenorhabditis elegans. *Mol. Cell. Endocrinol.* **299**, 51–57 (2009).
30. Piñero González, J., Carrillo Farnés, O., Vasconcelos, A. T. R. & González Pérez, A. Conservation of key members in the course of the evolution of the insulin signaling pathway. *Biosystems* **95**, 7–16 (2009).
31. Li, W., Kennedy, S. G. & Ruvkun, G. daf-28 encodes a C. elegans insulin superfamily member that is regulated by environmental cues and acts in the DAF-2 signaling pathway. *Genes Dev.* **17**, 844–858 (2003).
32. Pierce, S. B. *et al.* Regulation of DAF-2 receptor signaling by human insulin and ins-1, a member of the unusually large and diverse C. elegans insulin gene family. *Genes Dev.* **15**, 672–686 (2001).
33. Liu, J. *et al.* Insulin activates the insulin receptor to downregulate the PTEN tumour suppressor. *Oncogene* **33**, 3878–3885 (2014).
34. Hung, W. L. *et al.* Attenuation of insulin signalling contributes to FSN-1-mediated regulation of synapse development. *EMBO J.* **32**, 1745–1760 (2013).
35. Hung, W. L., Wang, Y., Chitturi, J. & Zhen, M. A *Caenorhabditis elegans* developmental decision requires insulin signaling-mediated neuron-intestine communication. *Development* **141**, 1767–1779 (2014).
36. Fernandes de Abreu, D. A. *et al.* An insulin-to-insulin regulatory network orchestrates phenotypic specificity in development and physiology. *PLoS Genet.* **10**, e1004225 (2014).
37. Murphy, C. T. Insulin/insulin-like growth factor signaling in C. elegans. *WormBook* 1–43 (2013) doi:10.1895/wormbook.1.164.1.
38. Paradis, S. & Ruvkun, G. Caenorhabditis elegans Akt/PKB transduces insulin receptor-like signals from AGE-1 PI3 kinase to the DAF-16 transcription factor. *Genes Dev.* **12**, 2488–2498 (1998).
39. Paradis, S., Ailion, M., Toker, A., Thomas, J. H. & Ruvkun, G. A PDK1 homolog is necessary and sufficient to transduce AGE-1 PI3 kinase signals that regulate diapause in Caenorhabditis elegans. *Genes Dev.* **13**, 1438–1452 (1999).

40. Libina, N., Berman, J. R. & Kenyon, C. Tissue-Specific Activities of C. elegans DAF-16 in the Regulation of Lifespan. *Cell* **115**, 489–502 (2003).
41. Henderson, S. T. & Johnson, T. E. daf-16 integrates developmental and environmental inputs to mediate aging in the nematode Caenorhabditis elegans. *Curr. Biol. CB* **11**, 1975–1980 (2001).
42. Lee, R. Y., Hench, J. & Ruvkun, G. Regulation of C. elegans DAF-16 and its human ortholog FKHRL1 by the daf-2 insulin-like signaling pathway. *Curr. Biol. CB* **11**, 1950–1957 (2001).
43. Byrne, A. B. *et al.* Insulin/IGF1 Signaling Inhibits Age-Dependent Axon Regeneration. *Neuron* **81**, 561–573 (2014).
44. Roy, C. *et al.* DAF-2/insulin IGF-1 receptor regulates motility during aging by integrating opposite signaling from muscle and neuronal tissues. *Aging Cell* **21**, (2022).
45. Dixon, S. J., Alexander, M., Chan, K. K. M. & Roy, P. J. Insulin-like signaling negatively regulates muscle arm extension through DAF-12 in Caenorhabditis elegans. *Dev. Biol.* **318**, 153–161 (2008).
46. Oh, K. H. & Kim, H. Reduced IGF signaling prevents muscle cell death in a *Caenorhabditis elegans* model of muscular dystrophy. *Proc. Natl. Acad. Sci.* **110**, 19024–19029 (2013).
47. Momma, K., Homma, T., Isaka, R., Sudevan, S. & Higashitani, A. Heat-Induced Calcium Leakage Causes Mitochondrial Damage in *Caenorhabditis elegans* Body-Wall Muscles. *Genetics* **206**, 1985–1994 (2017).
48. Zhang, P., Judy, M., Lee, S.-J. & Kenyon, C. Direct and Indirect Gene Regulation by a Life-Extending FOXO Protein in C. elegans: Roles for GATA Factors and Lipid Gene Regulators. *Cell Metab.* **17**, 85–100 (2013).
49. Murphy, C. T. *et al.* Genes that act downstream of DAF-16 to influence the lifespan of Caenorhabditis elegans. *Nature* **424**, 277–283 (2003).
50. McElwee, J., Bubb, K. & Thomas, J. H. Transcriptional outputs of the Caenorhabditis elegans forkhead protein DAF-16. *Aging Cell* **2**, 111–121 (2003).
51. Lee, S.-J., Murphy, C. T. & Kenyon, C. Glucose Shortens the Life Span of C. elegans by Downregulating DAF-16/FOXO Activity and Aquaporin Gene Expression. *Cell Metab.* **10**, 379–391 (2009).
52. Kaplan, R. E. W. *et al.* dbl-1/TGF-β and daf-12/NHR Signaling Mediate Cell-Nonautonomous Effects of daf-16/FOXO on Starvation-Induced Developmental Arrest. *PLOS Genet.* **11**, e1005731 (2015).
53. Hibshman, J. D. *et al.* daf-16/FoxO promotes gluconeogenesis and trehalose synthesis during starvation to support survival. *eLife* **6**, e30057 (2017).
54. Kaletsky, R. *et al.* The C. elegans adult neuronal IIS/FOXO transcriptome reveals adult phenotype regulators. *Nature* **529**, 92–96 (2016).
55. Kudron, M. M. *et al.* The ModERN Resource: Genome-Wide Binding Profiles for Hundreds of Drosophila and Caenorhabditis elegans Transcription Factors. *Genetics* **208**, 937–949 (2018).
56. Schuster, E. *et al.* DamID in *C. elegans* reveals longevity-associated targets of DAF-16/FoxO. *Mol. Syst. Biol.* **6**, 399 (2010).
57. Tepper, R. G. *et al.* PQM-1 Complements DAF-16 as a Key Transcriptional Regulator of DAF-2-Mediated Development and Longevity. *Cell* **154**, 676–690 (2013).
58. Blum, M. *et al.* The InterPro protein families and domains database: 20 years on. *Nucleic Acids Res.* **49**, D344–D354 (2021).

59. Fares, H. & Greenwald, I. Genetic Analysis of Endocytosis in Caenorhabditis elegans: Coelomocyte Uptake Defective Mutants. *Genetics* **159**, 133–145 (2001).
60. Cohen, M. *et al.* Coordinated regulation of foraging and metabolism in C. elegans by RFamide neuropeptide signaling. *Cell Metab.* **9**, 375–385 (2009).
61. De Rosa, M. J. *et al.* The flight response impairs cytoprotective mechanisms by activating the insulin pathway. *Nature* **573**, 135–138 (2019).
62. Suh, J. & Hutter, H. A survey of putative secreted and transmembrane proteins encoded in the C. elegans genome. *BMC Genomics* **13**, 333 (2012).
63. Zhao, Y. *et al.* Mutation of daf-2 extends lifespan via tissue-specific effectors that suppress distinct life-limiting pathologies. *Aging Cell* **20**, e13324 (2021).
64. Wu, C.-Y. *et al.* Enhancing GABAergic Transmission Improves Locomotion in a Caenorhabditis elegans Model of Spinal Muscular Atrophy. *eNeuro* **5**, ENEURO.0289-18.2018 (2018).
65. Zheng, Z. *et al.* GABAergic synapses suppress intestinal innate immunity via insulin signaling in Caenorhabditis elegans. *Proc. Natl. Acad. Sci. U. S. A.* **118**, e2021063118 (2021).
66. Chen, L. *et al.* Escape steering by cholecystokinin peptidergic signaling. *Cell Rep.* **38**, 110330 (2022).
67. Li, C. Neuropeptides. *WormBook* 1–36 (2008) doi:10.1895/wormbook.1.142.1.
68. Alkon, D. L., Nelson, T. J., Zhao, W. & Cavallaro, S. Time domains of neuronal Ca2+ signaling and associative memory: steps through a calexcitin, ryanodine receptor, K+ channel cascade. *Trends Neurosci.* **21**, 529–537 (1998).
69. Nelson, T. J. *et al.* Calexcitin interaction with neuronal ryanodine receptors. 11 (1999).
70. Nelson, T. J. *et al.* Calexcitin: a signaling protein that binds calcium and GTP, inhibits potassium channels, and enhances membrane excitability. *Proc. Natl. Acad. Sci. U. S. A.* **93**, 13808–13813 (1996).
71. Gombos, Z., Jeromin, A., Mal, T. K., Chakrabartty, A. & Ikura, M. Calexcitin B Is a New Member of the Sarcoplasmic Calcium-binding Protein Family. *J. Biol. Chem.* **276**, 22529–22536 (2001).
72. Gordus, A., Pokala, N., Levy, S., Flavell, S. W. & Bargmann, C. I. Feedback from network states generates variability in a probabilistic olfactory circuit. *Cell* **161**, 215–227 (2015).
73. Sordillo, A. & Bargmann, C. I. Behavioral control by depolarized and hyperpolarized states of an integrating neuron. *eLife* **10**, e67723 (2021).
74. Jin, X., Pokala, N. & Bargmann, C. I. Distinct Circuits for the Formation and Retrieval of an Imprinted Olfactory Memory. *Cell* **164**, 632–643 (2016).
75. Brenner, S. The genetics of Caenorhabditis elegans. *Genetics* **77**, 71–94 (1974).
76. Mello, C. & Fire, A. DNA transformation. *Methods Cell Biol.* **48**, 451–482 (1995).
77. Ji, N. *et al.* Corollary discharge promotes a sustained motor state in a neural circuit for navigation. *eLife* **10**, e68848 (2021).
78. Spencer, W. C. *et al.* Isolation of Specific Neurons from C. elegans Larvae for Gene Expression Profiling. *PLOS ONE* **9**, e112102 (2014).
79. Hoogewijs, D., Houthoofd, K., Matthijssens, F., Vandesompele, J. & Vanfleteren, J. R. Selection and validation of a set of reliable reference genes for quantitative sod gene expression analysis in C. elegans. *BMC Mol. Biol.* **9**, 9 (2008).
80. Schindelin, J. *et al.* Fiji: an open-source platform for biological-image analysis. *Nat. Methods* **9**, 676–682 (2012).

Figure 1

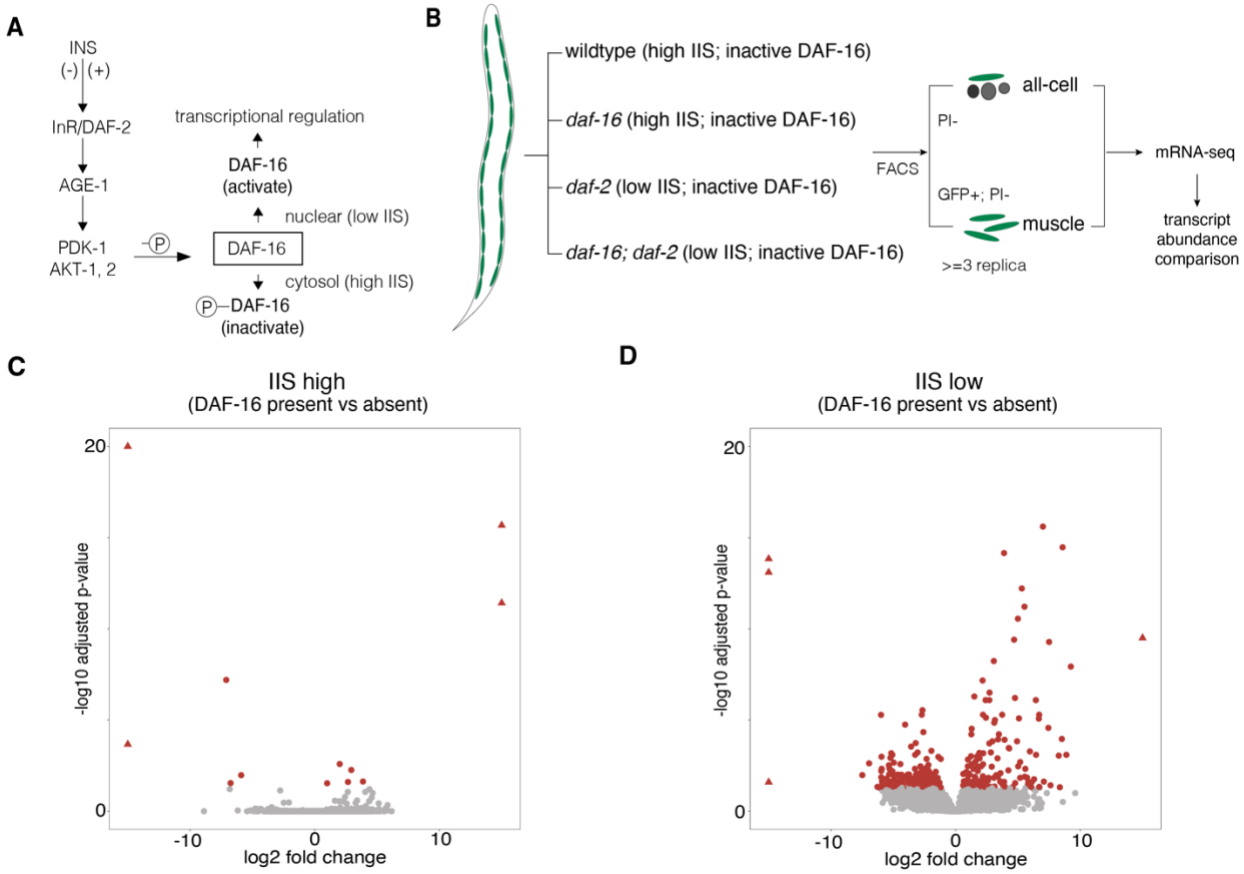

Figure 1. DAF-16 activity in different genetic backgrounds. (A) The effect of insulin/IGF-1 signaling (IIS) on DAF-16 activity. A schematic of the IIS pathway in *C. elegans* is shown. Phosphorylation of DAF-16 sequesters the FOXO transcription factor from the nucleus, inhibiting DAF-16-directed transcriptional regulation. (B) Schematic of FACS/mRNA-seq pipeline for data collection. Animals of different genotypes (wild-type, *daf-16(lf)*, *daf-2(lf)*, *daf-16(lf); daf-2(lf)*) express GFP in muscles. Young adults were collected, and cells were dissociated before being subjected to FACS analysis. GFP+ but propidium negative (PI-) cells were collected as muscle cells whereas GFP and PI- cells were collected as all cell controls. Total mRNA was isolated for sequencing. (C-D) Differentially expressed genes between wild-type muscle cells and *daf-16(lf)* muscle cells (C) and between *daf-2(lf)* muscle cells and *daf-2(lf); daf-16(lf)* muscle cells (D). Red dots indicate genes with FDR < 0.05.

Figure 2

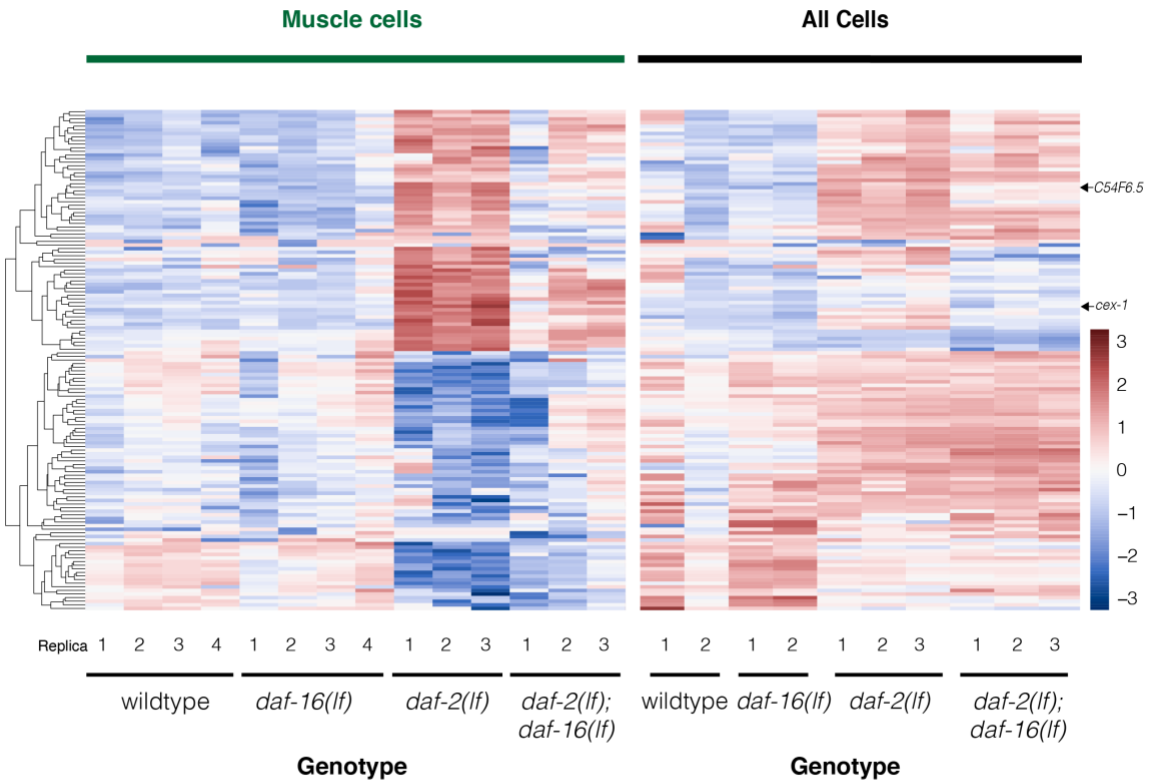

Figure 2. Differential gene expression analysis across eight transcriptomes. Heatmap of gene abundance of the 139 candidate genes for muscle-specific DAF-16-dependent transcriptional changes. (Left) Candidate gene abundance in muscle cells; (Right) Candidate gene abundance in 'all cells', compared between four genetic backgrounds: wild-type, *daf-16(lf)*, *daf-2(lf)*, and *daf-2(lf); daf-16(lf)*. Candidates are hierarchically clustered by similarities. Colors correspond to the z-score normalized over the average abundance of each gene across all samples.

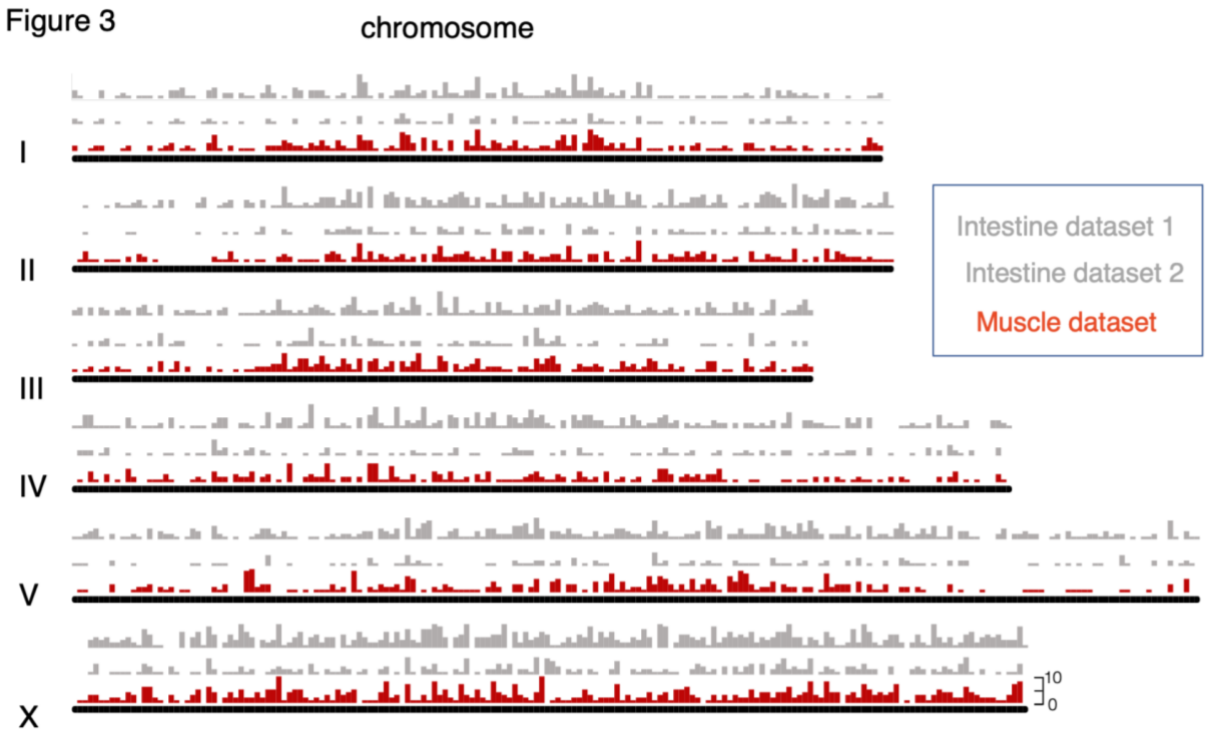

Figure 3. DAF-16 binding sites in the muscle and intestinal cells. Mapped DAF-16a docking sites per chromosome, including two datasets for intestine ChIP-seq (grey) and one dataset for muscle ChIP-seq (red). The numbers of peaks are binned for every 100 thousand base pairs.

Figure 4

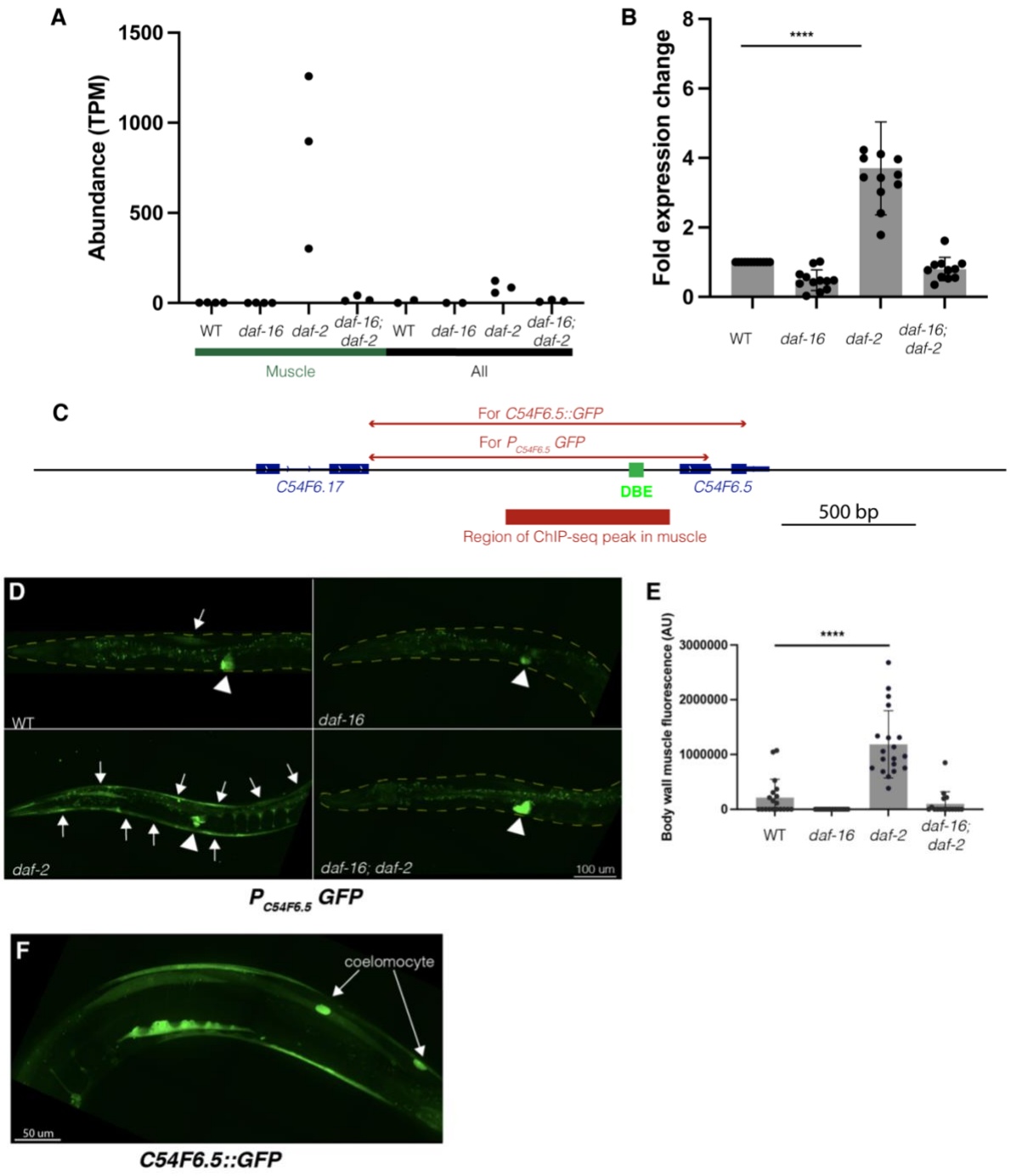

Figure 4. Muscle-specific upregulation of *C54F6.5* by DAF-16. (A) *C54F6.5* gene abundance across genetic backgrounds and cell types. (B) Fold changes of *C54F6.5* expression in respective genetic backgrounds, normalized against wildtype level by RT-qPCR. Error bars: standard deviation. (C) The genomic structure of *C54F6.5*. Sequences labeled by the red bars are included in the transcriptional and translational reporters. The location of the DAF-16 binding element (DBE) is indicated. (D) Representative confocal images of the *C54F6.5* transcriptional reporter in different genetic backgrounds. Arrows and arrowheads denote muscles and spermathecae, respectively. (E) Quantification of muscle GFP intensity. **** $p < 0.0001$. Error bars: Standard Deviation. (F) Representative confocal images of the *C54F6.5* translational reporter, in muscles and coelomocytes.

Figure 5

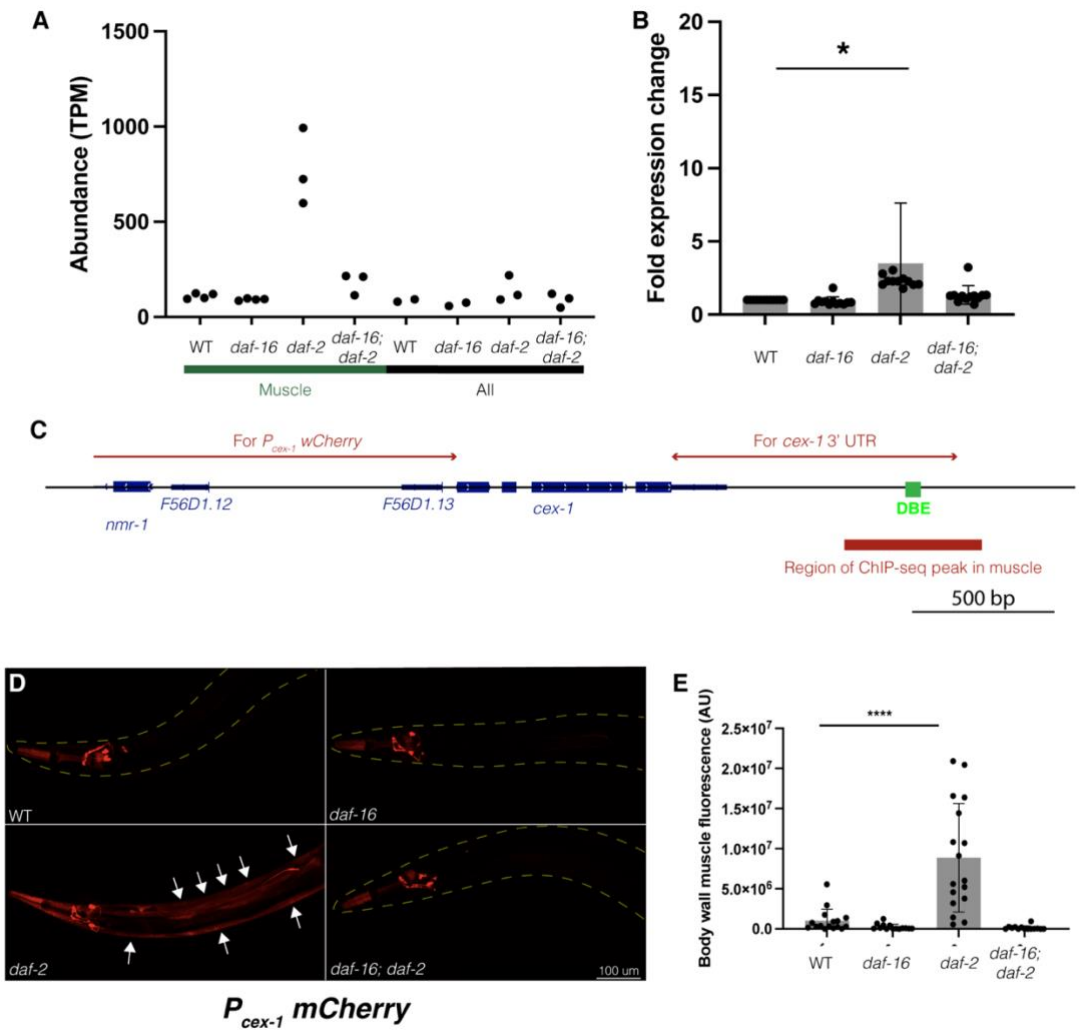

Figure 5. Muscle-specific upregulation of *cex-1* by DAF-16. (A) *cex-1* gene abundance across genetic backgrounds and cell types. (B) Fold changes of *cex-1*, normalized against the wild-type level by mRNA-RT-qPCR. * $p < 0.5$. Error bars: SD. (C) The genomic locus of *cex-1*. Red bars mark the genomic sequences included for the *cex-1* transcriptional reporter. Only a partial downstream sequence, including the DAF-16 binding element (DBE), is shown. (D) Representative confocal images of the *cex-1* transcriptional reporter. Arrows and arrowheads denote muscle cells and the pair of RIM interneurons, respectively. (E) Quantification of muscle-specific reporter intensity. **** $p < 0.0001$. Error bars: SD.

Table 1. Candidate genes of DAF-16-dependent transcriptional regulation under the high IIS state

	Salmon muscle CPM (mean±SD, n=4)		STAR-HTSeq muscle CPM (mean±SD, n=4)		DESeq2 based on Salmon	
Gene	**wildtype**	***daf-16***	**wildtype**	***daf-16***	**log2 fold change**	**adjusted p-value**
gcy-3	0.02±0.03	0±0	0.02±0.02	0±0	17.27	2.11E-16
F23B2.10	0.01±0.02	0±0	0.03±0.04	0±0	15.99	3.82E-12
flr-4	0.86±1.15	0.05±0.03	0.89±1.24	0.08±0.07	3.87	2.34E-02
C55C3.3	3.57±2.17	0.49±0.40	3.93±2.51	0.51±0.39	2.93	5.47E-03
fpn-1.2	0.54±0.43	0.08±0.03	0.66±0.38	0.08±0.04	2.67	2.48E-02
ZK105.1	15.86±7.03	4.06±2.11	18.27±6.84	4.59±1.98	2.00	2.58E-03
C10F3.7	0.03±0.04	3.63±6.49	0.02±0.04	3.62±6.42	-5.90	1.05E-02
srbc-15	0.01±0.02	2.17±2.99	0.01±0.02	1.86±2.41	-6.75	2.86E-02
col-33	0.16±0.15	30.53±46.51	0.17±0.16	34.47±52.29	-7.10	6.32E-08
Y6B3B.1	0±0	0.07±0.12	0±0	0.06±0.11	-17.86	1.67E-23
fbxb-33	0±0	1.75±3.48	0±0	0.01±0.01	-28.14	2.15E-04
**** daf-16***	**23.08±6.49**	**11.30±8.73**	**24.17±6.70**	**11.74±8.99**	**0.99**	**2.92E-02**

*: Excluded from the gene list for DAF-16-dependent transcriptional regulation. Reduced reads here resulted from the loss of transcription in the deleted genomic region in the *daf-16(mu86)* allele used in this study.

Table 2. A summary of the sequential criteria for muscle-specific and DAF-16-direct transcriptional targets

Number of candidates	Description	Criteria (adjusted p-value < 0.05 between)
195 *	DAF-16-dependent transcriptional changes observed in muscle cells	Muscle samples: *daf-2* vs wildtype, *daf-16*, *daf-16; daf-2*
139 **	DAF-16-dependent transcriptional changes enriched for muscle cells	+ *daf-2* muscles vs wildtype, *daf-16*, *daf-2*, *daf-2; daf-16* all cells
55 ***	Muscle-enriched DAF-16-dependent transcriptional change with direct DAF-16 binding	+ with DAF-16a binding within 5kb of the CDS in the muscle cells
14 ****	Candidate muscle-specific DAF-16 direct targets	+ without DAF-16a binding in the intestinal cells

*: See Table S1 for the gene list.
**: See Table S2 for the gene list.
***: See Table S3 for the gene list.
****: See Table 3 for the gene list.

Table 3. Fourteen candidate muscle-specific direct DAF-16 transcriptional targets.

	Salmon muscle CPM (mean±SD, n=3)		**STAR-HTSeq muscle CPM (mean±SD, n=3)**		**DESeq2 based on Salmon**	
Gene	***daf-2***	***daf-16; daf-2***	***daf-2***	***daf-16; daf-2***	**log2 fold change**	**adjusted p-value**
alh-2	1.95±2.44	0±0	2.24±2.88	0±0	8.88	8.06E-04
C54F6.5*	**30.63±17.11**	**0.84±0.51**	**32.82±17.93**	**0.87±0.55**	**5.52**	**6.10E-12**
cex-1*	**737.98±235.3**	**168.9±38.31**	**771.67±254.42**	**173.65±41.31**	**2.40**	**8.08E-07**
gstk-2	23.32±3.34	5.03±0.82	22.01±3.94	5.39±0.82	2.33	4.56E-02
mlcd-1	29.8±3.52	11.91±5.59	26.39±3.56	10.72±5.07	1.72	9.91E-04
act-2	940.04±471.42	386.24±130.45	749.3±375.8	298.78±102.85	1.59	1.90E-03
F23D12.7	105.27±24.15	46.76±11.32	110.53±25.16	47.56±11.5	1.29	4.52E-02
tiar-3	45.43±11.5	22.35±4.81	49.41±12	23.71±5.69	1.29	2.65E-03
Y43F8B.1	1475.99±257.45	677.98±58.46	1547.34±272.86	695.17±62.1	1.20	4.39E-02
unc-78	338.08±17.49	200.69±36.39	351.32±20.26	204.05±38.8	0.97	2.44E-02
ksr-1	29.31±10.06	17.7±3.00	30.5±10.45	17.93±3.11	0.97	4.02E-02
aqp-2	585.75±155.07	414.25±114.85	606.98±154.31	421.93±120.2	0.78	4.79E-02
goa-1	225.55±42.3	172.71±45.62	235.42±46.7	176.81±48.57	0.66	3.78E-02
rap-3	0.01±0.02	0.4±0.24	0.01±0.02	0.41±0.2	-4.95	1.15E-02

*: high-confidence candidates.

Supplemental data and tables

Figure S1

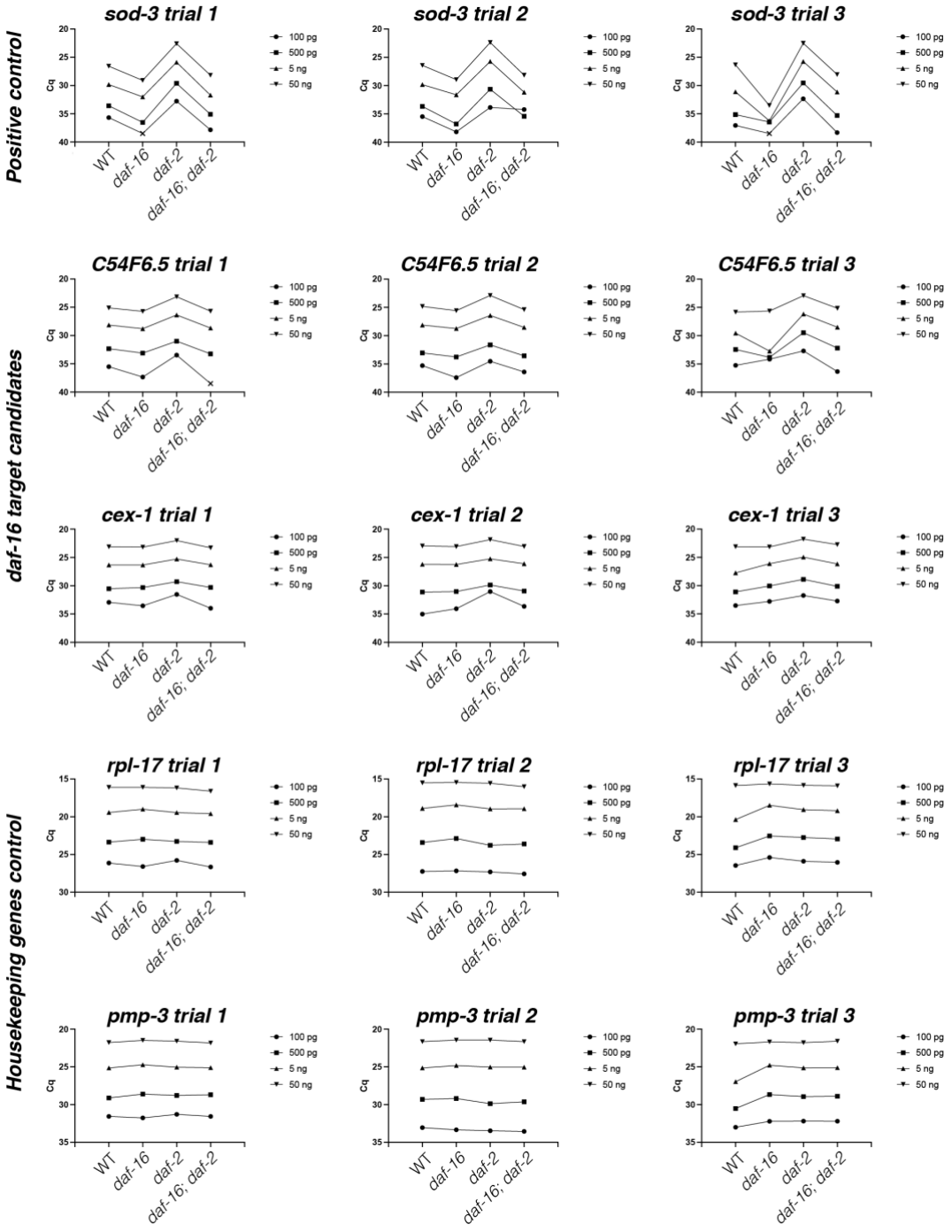

Figure S1: Raw Cq values for 3 RT-qPCR replicas. RT-qPCR was performed for *C54F6.5*, *cex-1*, *sod-3* (positive control), and *rpl-17* and *pmp-3* (housekeeping gene controls) at different concentrations. *daf-2(lf)* showed consistent trends of transcript increase for *sod-3*, *C54F6.5* and *cex-1*, but not for the *rpl-17* and *pmp-3* housekeeping genes.

Figure S2

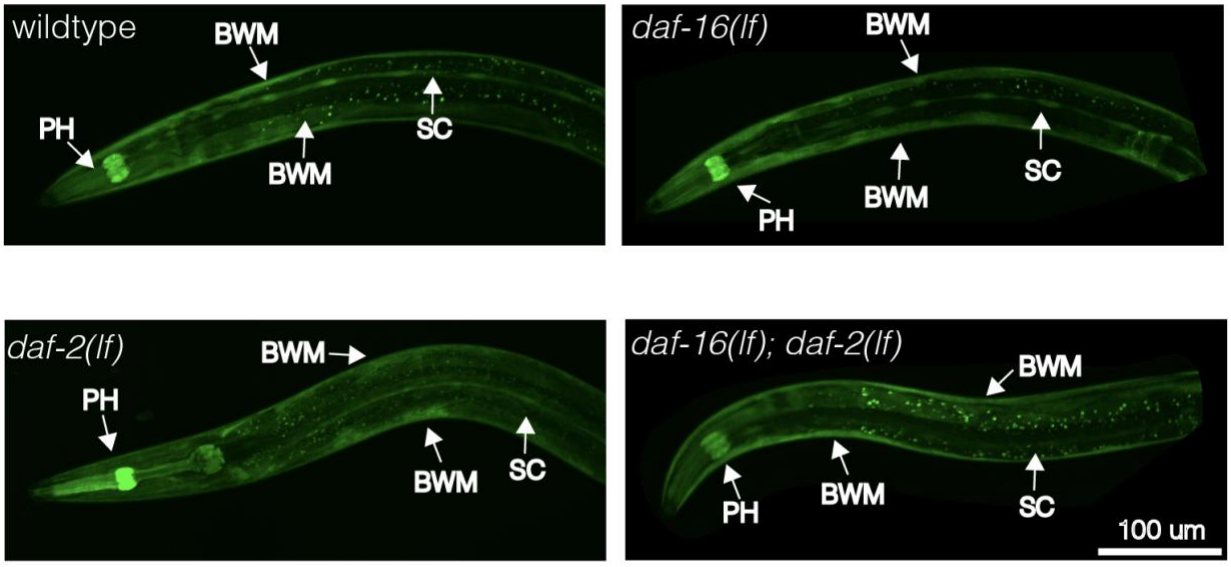

Figure S2. Expression of the *gstk-2* reporter does not show dependence on DAF-16. The expression pattern of an endogenously expressed *gstk-2::*SL2::mNeonGreen reporter showed a similar expression pattern in the body wall muscle (BWM), pharynx (PH), and seam cells (SC) across wildtype, *daf-16(lf)*, *daf-2(lf)*, and *daf-2(lf); daf-16(lf)* animals.

Table S1. A list of 195 candidates filtered by the first criterion described in Table 2.

Table S2. A list of 139 candidates filtered by the second criterion described in Table 2.

Table S3. A list of 55 candidates filtered by the third criterion described in Table 2.

Table S4. A list of strains used in this study.

Strain	Genotype	Notes
N2	wildtype	
CF1038	*daf-16(mu86)* I	
CB1370	*daf-2(e1370)* III	
XE1464	*daf-16(mu86)* I; *daf-2(e1370)* III; *wpSi9 [Pspl-1 GFP::daf-16a + Cbr-unc-119(+)]*	for intestine ChIP-seq
ZM7247	*daf-16(mu86)* I; *daf-2(e1370)* III; *hpSi4 [Pmyo-3 GFP::daf-16a]*	for muscle ChIP-seq
ZM8745	*daf-16(mu86)* I; *daf-2(e1370)* III; *hpSi15 [Pges-1 GFP::daf-16a]*	for intestine ChIP-seq
JAC127	*csbIs6 [Pmyo-3 GFP::rpl-1]*	for wild-type mRNA-seq
ZM9156	*daf-16(mu86)* I; *csbIs6 [Pmyo-3 GFP::rpl-1]*	for *daf-16* mRNA-seq
ZM10379	*daf-16(mu86)* I; *daf-2(e1370)* III; *csbIs6 [Pmyo-3 GFP::rpl-1]*	for *daf-16; daf-2* mRNA-seq
ZM10380	*daf-2(e1370)* III; *csbIs6 [Pmyo-3 GFP::rpl-1]*	for *daf-2* mRNA-seq
ZM11295	*hpEx4481 [PC54F6.5 GFP + Pmyo-2 RFP]*	*C54F6.5* transcriptional reporter
ZM11296	*daf-16(mu86)* I; *hpEx4481 [PC54F6.5 GFP + Pmyo-2 RFP]*	*C54F6.5* transcriptional reporter
ZM11297	*daf-2(e1370)* III; *hpEx4481 [PC54F6.5 GFP + Pmyo-2 RFP]*	*C54F6.5* transcriptional reporter
ZM11298	*daf-16(mu86)* I; *daf-2(e1370)* III; *hpEx4481 [PC54F6.5 GFP + Pmyo-2 RFP]*	*C54F6.5* transcriptional reporter
ZM11333	*daf-2(e1370)* III; *hpEx4491 [C54F6.5::GFP + Pmyo-2 RFP]*	*C54F6.5* translational reporter
ZM11338	*hpEx4489 [Pcex-1 mCherry cex-1-3' UTR + Pttx-3 GFP]*	*cex-1* transcriptional reporter with *cex-1* 3' UTR
ZM11339	*daf-16(mu86)* I; *hpEx4489 [Pcex-1 mCherry cex-1-3' UTR + Pttx-3 GFP]*	*cex-1* transcriptional reporter with *cex-1* 3' UTR
ZM11340	*daf-2(e1370)* III; *hpEx4489 [Pcex-1 mCherry cex-1-3' UTR + Pttx-3 GFP]*	*cex-1* transcriptional reporter with *cex-1* 3' UTR
ZM11341	*daf-16(mu86)* I; *daf-2(e1370)* III; *hpEx4489 [Pcex-1 mCherry cex-1-3' UTR + Pttx-3 GFP]*	*cex-1* transcriptional reporter with *cex-1* 3' UTR
PHX5762	*gstk-2(syb5762)* IV	*gstk-2::SL2::GFP CRISPR/Cas9 reporter*
ZM11354	*daf-16(mu86)* I; *gstk-2(syb5762)* IV	*gstk-2::SL2::GFP CRISPR/Cas9 reporter*
ZM11349	*daf-2(e1370)* III; *gstk-2(syb5762)* IV	*gstk-2::SL2::GFP CRISPR/Cas9 reporter*
ZM11350	*daf-16(mu86)* I; *daf-2(e1370)* III; *gstk-2(syb5762)* IV	*gstk-2::SL2::GFP CRISPR/Cas9 reporter*

Table S5. A list of RT-qPCR primers used in this study.

sod-3	OZM6628	CTAAGGATGGTGGAGAACCTTCA
	OZM6629	CGCGCTTAATAGTGTCCATCAG
C54F6.5	OZM6630	TGTTCACCAAGACCCTCCTC
	OZM6631	TTGCAGTTTCTACACGTCACG
cex-1	OZM6632	TCCGATGTTGATCCGTTCCT
	OZM6633	CACGGACTTTCTTGACAACCA
pmp-3	OZM6669	GTTCCCGTGTTCATCACTCAT
	OZM6670	ACACCGTCGAGAAGCTGTAGA
rpl-17	OZM6671	AGTACAAGGGGCTCGATGTTG
	OZM6672	TGGGGAAGACATGTATGGGTTG